J. Biochem. 119, 1045-1055 (1996)

Secondary Structure and Ca^{2+}-Binding Property of the N-Terminal Half Domain of Calmodulin from Yeast *Saccharomyces cerevisiae* as Studied by NMR[1]

Shin-ya Ohki,* Kazunori Miura,† Moyoko Saito,† Ken-ichi Nakashima,‡ Hironobu Maekawa,‡ Michio Yazawa,‡ Sakae Tsuda,§ and Kunio Hikichi*,[2]

*High-Resolution NMR Laboratory, †Divisions of Biological Sciences and ‡Chemistry, Graduate School of Science, Hokkaido University, N10-W8, Kita-ku, Sapporo 060; and §Bioscience and Chemistry Division, Hokkaido National Industrial Research Institute, 2-17-2-1 Tsukisamu-higashi, Toyohira-ku, Sapporo 062

Received for publication, December 8, 1995

Using two- and three-dimensional NMR techniques, ^1H and main-chain ^{15}N resonances of the N-terminal half domain of yeast calmodulin (YCM0-N) in the presence of Mg^{2+} and Ca^{2+} (Mg^{2+}- and Ca^{2+}-forms) were assigned. The secondary structures of YCM0-N in both forms were determined. The NOESY and ^{15}N-edited NOESY spectra of YCM0-N in each form indicate that there is a hydrophobic core and that two Ca^{2+}-binding loops are connected by a short antiparallel β-sheet. There are four helices (A, B, C, and D named from the N-terminus) for YCM0-N in the Mg^{2+}-form. The B-helix is, however, not formed in the Ca^{2+}-form. The Ca^{2+}-binding of YCM0-N was monitored by (^1H,^{15}N)-HSQC at various Ca^{2+} concentrations. The observed spectral changes as a function of Ca^{2+}-concentration can not readily be grouped into a small number of classes; each residue shows individual spectral change. There is no apparent relationship between the spectral change and the type or location of the amino acid concerned.

Key words: Ca^{2+}-induced conformational change, NMR, N-domain of yeast calmodulin, secondary structure.

Calmodulin (CaM), a small Ca^{2+}-binding protein, is widely distributed in eukaryotic cells. Amino acid sequences of CaM from various sources are highly conservative. CaM acts as a primary intracellular receptor of Ca^{2+} signaling. CaM interacts with and activates targets in a Ca^{2+}-dependent manner (see Ref. *1* and references cited therein).

X-Ray crystallographic studies have shown that Ca^{2+}-saturated CaM from several sources has a dumbbell-like structure (*2-4*). Each of two globular domains (N- and C-domains) connected by a long α-helix binds two Ca^{2+} ions. The four Ca^{2+}-binding sites (numbered I to IV from the N-terminus) consist of helix-loop-helix motives in the "EF-hand" structure and six residues in the loop contribute to Ca^{2+}-binding (*5*). The eight helix regions of four EF-hand motives in CaM are named A to H from the N-terminus (*2*). A short antiparallel β-sheet links the two Ca^{2+}-binding sites in each domain, which has a hydrophobic core on the surface for target binding.

Recent NMR studies showed that apo-CaM is very similar to Ca^{2+}-saturated CaM in respect of secondary structural elements (*6-9*). However, Ca^{2+}-binding induces a change in the disposition of secondary structural elements; the pairs of B- and C-helices and F- and G-helices in each domain move away from the hydrophobic core in such a way that the hydrophobic core in each domain is exposed to the solvent and available for target binding.

It has been shown that CaM interacts with Mg^{2+} and assumes a characteristic conformation (Mg^{2+}-form) which is different from those of the apo- and Ca^{2+}-saturated forms (binding constant $K_a \geq 10^3\ M^{-1}$; *10-13*). Concentrations of CaM and Mg^{2+} in cells are $3\text{-}20\times10^{-6}$ M and more than 10^{-3} M, respectively. We reported that Mg^{2+} suppresses the formation of the active complex, $4Ca^{2+}$-CaM-target, at lower Ca^{2+} concentrations (*14, 15*). Therefore, CaM in the Mg^{2+}-form is thought to be in the inactive state.

Physicochemical properties of CaM isolated from the yeast *Saccharomyces cerevisiase* (yCaM; 146 amino acid residues) are mostly similar to those of other CaMs in

[1] This work was partly supported by a Grant-in-Aid (No. 06276202) from the Ministry of Education, Science, Sports and Culture of Japan.
[2] To whom correspondence should be addressed. Phone: +81-11-706-2770, Fax: +81-11-716-4093, E-mail: hikichi@luna.polymer.hokudai.ac.jp

Abbreviations: 1D, one-dimensional; 2D, two-dimensional; 3D, three-dimensional; CaM, calmodulin; CD, circular dichroism; CSI, chemical-shift index; DANTE, delays alternating with nutation for tailored excitation; DQF-COSY, double quantum filtered correlation spectroscopy; HMQC, hetero nuclear multiple quantum coherence spectroscopy; HSQC, hetero nuclear single quantum coherence spectroscopy; NMR, nuclear magnetic resonance; NOE, nuclear Overhauser effect; NOESY, nuclear Overhauser effect spectroscopy; PFG, pulsed field gradient; SR1331, self-refocused 1331; TOCSY, total correlation spectroscopy; TSP, 2,2,3,3-tetradeutero-3-(trimethylsilyl)propionic acid sodium salt; YCM0-N, N-terminal half domain of yeast calmodulin; $d_{NN}(i-1,i)$, NOE cross-peak between amide protons of residues $i-1$ and i; $d_{N\alpha}/d_{\alpha N}$, ratio of two NOE cross-peak intensities between amide and α proton of residue i [$d_{N\alpha}(i,i)$] and between α proton of residue $i-1$ and amide proton of residue i [$d_{\alpha N}(i-1,i)$]; $d_{\alpha N}(i-3,i)$, NOE cross-peak between α proton of residue $i-3$ and amide proton of residue i; $d\beta_N(i-1,i)$, NOE cross-peak between β proton of residue $i-1$ and amide proton of residue i; yCaM, yeast calmodulin.

respect of heat-stability, acidicity, and Ca^{2+}-dependent binding of hydrophobic molecules (*16-22*). However, yCaM shares only 60% homology in amino acid sequence with vertebrate CaMs (*16*).

The 61st residue in Ca^{2+}-binding site II of yCaM is His in place of the highly conserved Gly. The 66th residue in Ca^{2+}-binding site II of yCaM is Ser; it is Pro in vertebrate CaM. In the region corresponding to site IV of vertebrate CaM, two residues are deleted and a Gln residue is substituted for the conserved Glu at the end of the loop in the EF-hand. Site IV of yCaM does not bind Ca^{2+}; as a result, yCaM binds only three Ca^{2+} ions.

The biological role of yCaM in yeast has not been clarified yet. It is reported that yCaM activates targets of vertebrate CaM such as phosphodiesterase (PDE) and myosin light-chain kinase (MLCK), although the activity is not as high as that of vertebrate CaM (*18, 19*).

A previous NMR study showed that two fragments of yCaM, the 1st-77th and 75th-146th residues, retain the conformation in intact yCaM (*23*). The results suggest that yCaM is also in a dumbbell-like shape. The Ca^{2+}-binding properties of yCaM have been studied through a few separated signals in one-dimensional (1D) ^{1}H-NMR spectra. Far-UV CD studies indicated that the helix-content of yCaM is decreased by Ca^{2+}-binding, while that of vertebrate CaM is increased. Details of the structure and Ca^{2+}-induced conformational change of yCaM are not known yet.

In this paper we describe the secondary structure of the N-terminal half domain of yCaM (YCM0-N; 77 amino acid residues) in the Mg^{2+}- and Ca^{2+}-forms as determined by two-dimensional (2D) and three-dimensional (3D) NMR. We present the results of Ca^{2+}-titration of the ^{15}N-labeled YCM0-N monitored by sensitivity enhanced 2D-(^{1}H,^{15}N)-PFG-HSQC (*24*). We discuss the similarities and the differences between the Mg^{2+}- and Ca^{2+}-forms. The Ca^{2+}-form of YCM0-N is compared with that of vertebrate CaMs, and the Ca^{2+}-binding properties and Ca^{2+}-induced conformational change of YCM0-N are discussed.

MATERIALS AND METHODS

Sample Preparation—The N-terminal half domain of yCaM (YCM0-N; Ser1-Lys 77) was overexpressed in *Escherichia coli* TG1 carrying plasmid pYCM0-N, which was constructed from plasmid pYCM0 (*18, 19*) by substituting a stop codon, TGA, for TCA encoding Ser78 of the wild-type yCaM. Protein YCM0-N labeled uniformly with ^{15}N was obtained by growing the cells in M10 minimal medium with $^{15}NH_4Cl$ (1 g/1 liter; Isotec) (*25*). YCM0-N was purified by a slightly modified TCA precipitation method as described previously (*18, 19, 26*). We used a Sephadex G-25 gel column at the final step of purification in order to obtain metal-free YCM0-N. One liter of culture yielded about 12 mg of YCM0-N.

NMR Sample of Mg^{2+}-Form—Three NMR samples (a), (b), and (c) were prepared under the following conditions: (a) [YCM0-N] = 3 mM, [Mg^{2+}] = 300 mM, and [KCl] = 50 mM in D_2O at pH = 6.5-7.0 with 0.03% NaN_3, (b) [YCM0-N] = 3 mM, [Mg^{2+}] = 300 mM, and [KCl] = 50 mM in H_2O containing 10% D_2O at pH = 6.5-7.0 with 0.03% NaN_3, and (c) [^{15}N-YCM0-N] = 3 mM, [Mg^{2+}] = 300 mM, and [KCl] = 50 mM in H_2O containing 10% D_2O at pH = 6.5-7.0 with 0.03% NaN_3. Each sample was adjusted to a neutral pH value by adding KOD and/or DCl.

NMR Sample of Ca^{2+}-Form—Three NMR samples (a), (b), and (c) were prepared under the following conditions: (a) [YCM0-N] = 3 mM, [Ca^{2+}] = 9 mM, and [KCl] = 50 mM in D_2O pH = 6.5-7.0 with 0.03% NaN_3, (b) [YCM0-N] = 3 mM, [Ca^{2+}] = 9 mM, and [KCl] = 50 mM in H_2O containing 10% D_2O at pH = 6.5-7.0 with 0.03% NaN_3, and (c) [^{15}N-YCM0-N] = 3 mM, [Ca^{2+}] = 9 mM, and [KCl] = 50 mM in H_2O containing 10% D_2O at pH = 6.5-7.0 with 0.03% NaN_3. Each sample was adjusted to a neutral pH value by adding KOD and/or DCl.

NMR Experiments for Assignment—All NMR data were recorded on JEOL JNM-A500 and A600 spectrometers at ^{1}H frequencies of 500 and 600 MHz, respectively. Each spectrometer is equipped with a 5 mm ^{1}H{^{13}C,^{15}N}-triple-resonance probe-head with a *z*-axis gradient coil. Temperature was kept at 30±0.1°C throughout the experiments.

2D-NMR data of DQF-COSY (*27*), NOESY (mixing time = 100, 150, and 300 ms) (*28, 29*), and TOCSY (MLEV time = 75 ms) (*30, 31*) were collected with 512×1,024 complex points in the $t_1 \times t_2$ time domain. Water peak suppression was achieved by DANTE (*32*) for DQF-COSY and TOCSY, and by 1-1 echo (*33, 34*) or SR1331 (*35*) for NOESY.

3D-(^{1}H, ^{1}H, ^{15}N)-PFG-NOESY-HSQC (mixing time = 150 ms; abbreviated as ^{15}N-edited 3D-NOESY) (*24, 36*) data and 3D-(^{1}H, ^{1}H, ^{15}N)-PFG-TOCSY-HSQC (MLEV time = 75 ms; abbreviated as ^{15}N-edited 3D-TOCSY) (*24, 37*) data were recorded with 128×256×32 complex points in the $t_1(^1H) \times t_2(^1H) \times t_3(^{15}N)$ time domain using the 500 MHz spectrometer. Pulse widths of 90° for ^{1}H and ^{15}N were 7.85 and 27.5 μs, respectively. Spectral widths of ^{1}H and ^{15}N resonances were 6,990 and 1,600 Hz, respectively. Decoupling of ^{15}N resonance over a frequency range of 2,400 Hz was achieved by the MPF6 sequence (*38, 39*). Water peak suppression was performed by selective gaussian pulse.

NMR Data Processing—NMR data were processed by NMRPipe (*40*) and PIPP (*41*) programs running on an SGI Indigo2. The 2D-NMR (DQF-COSY, NOESY, and TOCSY) data were zero-filled to 2K×2K complex data points. A 30%-shifted or non-shifted sine-bell window function was applied to both dimensions. The 3D-NMR data were zero-filled to 512×1,024×64 (^{1}H×^{1}H×^{15}N) complex points. A 50%-shifted sine-bell window function was applied to the two ^{1}H dimensions and a 30%-shifted sine-square window function to the ^{15}N dimension. Chemical shifts of ^{1}H and ^{15}N resonances are reported from the internal standard TSP (0 ppm) and external standard acidic $^{15}NH_4Cl$ (24.93 ppm), respectively.

Ca^{2+}-Titration by HSQC—The sample used for Ca^{2+}-titration monitored by 2D-HSQC was prepared under the following conditions: [^{15}N-YCM0-N] = 3 mM, [Mg^{2+}] = 300 mM, and [KCl] = 50 mM, in H_2O containing 10% D_2O at pH = 6.5-7.0. Sensitivity enhanced 2D-(^{1}H,^{15}N)-PFG-HSQC spectra were observed at various concentrations of Ca^{2+} at a ^{1}H frequency of 500 MHz. Temperature was kept at 30±0.1°C. The selective gaussian pulse was used for solvent suppression. Decoupling of ^{15}N resonance was achieved by the MPF6 sequence (*38, 39*). Collected data points were 128×512 in the $t_1 \times t_2$ time domain.

RESULTS

Sequential Assignments—The sequence-specific assignment was performed by the standard method using the 2D and ^{15}N-edited 3D NMR data (*42, 43*). Connectivities between main-chain amide protons and α protons in fingerprint regions of 2D-DQF-COSY, 2D-TOCSY, and ^{15}N-edited 3D-TOCSY spectra were mostly identified. Spin systems were classified on the basis of connectivities between the main-chain and side-chain protons observed in 2D-TOCSY and ^{15}N-edited 3D-TOCSY spectra. The NOE connectivities, $d_{NN}(i-1,i)$, $d_{\alpha N}(i-1,i)$, and $d_{\beta N}(i-1,i)$ derived from NOESY and ^{15}N-edited 3D-NOESY spectra were used to link spin systems sequentially.

Figure 1 shows strips of 2D-NOESY slice planes at different ^{15}N chemical shifts of ^{15}N-edited 3D-NOESY spectra for Ca^{2+}-form YCM0-N. In each strip, NOE peaks between an amide proton and other protons are shown. Assignment was performed based on the combination of 2D- and 3D-spectra. The sequential connectivity from Glu45 to Leu51 is represented by lines [$d_{NN}(i-1,i)$] and dashed lines [$d_{\alpha N}(i-1,i)$]. The sequential connectivity between Glu47 and Val48 is justified by NOE $d_{NN}(i-1,i)$ and $d_{\beta N}(i-1,i)$, though an NOE $d_{\alpha N}(i-1,i)$ peak between Glu47 and Val48 is not observed in this figure. The NOE cross peak $d_{\alpha N}$ (*47, 48*) is observed in 2D-NOESY spectra (data not shown). Four NOE $d_{\alpha N}(i-3, i)$ cross peaks (Glu45-Val48, Ala46-Asn49, Glu47-Asp50, and Val48-Leu51) are observed, as indicated by arrows. The chemical shift values of YCM0-N in the Mg^{2+}- and Ca^{2+}-forms are summarized in Table I.

Strategy for Secondary Structure Determination—The secondary structure of YCM0-N was determined from the following three data sets. The first is the successive NOE connectivities $d_{\alpha N}(i-3, i)$, which are indicative of α-helix (*42, 43*). The second is CSI (chemical-shift index) (*44, 45*), which is the chemical-shift deviation of the α ^{1}H resonance from random-coil. Positive CSI suggests α-helix and negative CSI, β-strand. The third is $d_{N\alpha}(i, i)/d_{\alpha N}(i-1,i)$ ratio (*46*). A $d_{N\alpha}/d_{\alpha N}$ ratio greater than unity is indicative of α-helix, and a ratio less than unity, of β-strand.

Secondary Structure of YCM0-N in the Mg^{2+}-Form—Figure 2A shows the data for determination of the secondary structure of YCM0-N in the Mg^{2+}-form. Ser1 to Leu4 are not assignable. NOE $d_{\alpha N}(i-3, i)$ connectivities are successively observed from Glu6 to Phe19. For these residues the $d_{N\alpha}/d_{\alpha N}$ ratios are greater than unity, and the CSI values are positive except for the CSI of Phe12. Thus, we conclude that the region from Glu6 to Phe19 is in the α-helix form, that is, A-helix (the nomenclature used for vertebrate CaM). The CSI value of Phe12 is negative. Negative CSI of Phe residue at the center of A-helix has also been reported for troponin C, which is one of the EF-hand proteins (*46*).

The next series of successive NOE $d_{\alpha N}(i-3, i)$ connectivities are observed from Ala33 to Leu39. The CSI values are positive and the $d_{N\alpha}/d_{\alpha N}$ ratios are greater than unity throughout this region, which corresponds to B-helix. Because Ser29, Ser30, Glu31, and Leu32 are not assigned, the N-terminal end of B-helix is not determined.

The third series of characteristic NOE $d_{\alpha N}(i-3, i)$ connectivities are observed from Glu45 to Met52. The CSI values are mostly positive and the $d_{N\alpha}/d_{\alpha N}$ ratios are mostly greater than unity throughout this region. The residues from Glu45 to Met52 form the C-helix.

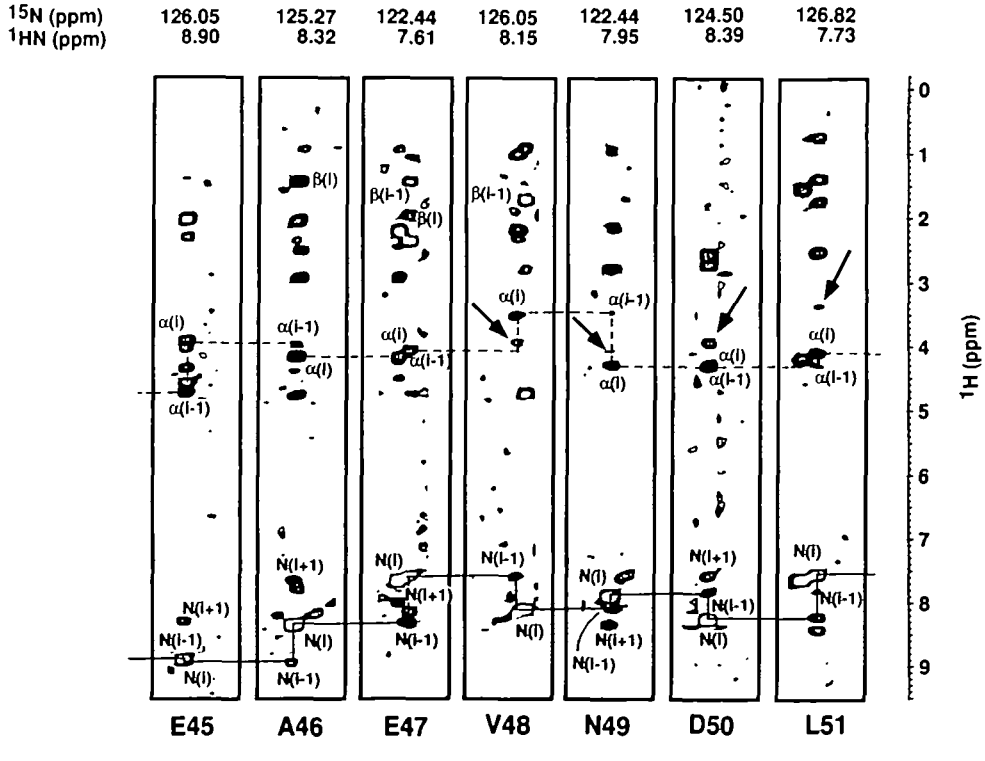

Fig. 1. **Strips of 2D-NOESY slice planes at different ^{15}N chemical shifts of 500 mHz ^{15}N-edited 3D-NOESY spectra at a mixing time of 150 ms at 30°C for Ca^{2+}-form YCM0-N.** Sample conditions are described in "MATERIALS AND METHODS." The ^{15}N chemical shift of the slice plane and the ^{1}HN chemical shift of the strip are shown at the top. N(i) represents the diagonal peak of amide proton. N(i+1) and N(i−1) represent NOE peaks of amide protons of the succeeding $d_{NN}(i, i+1)$ and preceding $d_{NN}(i-1, i)$ residues, respectively. $\alpha(i)$ represents the NOE cross peaks between ^{1}HN and α ^{1}H in the same residue [$d_{N\alpha}(i, i)$]; $\alpha(i-1)$ between ^{1}HN and α ^{1}H of the preceding residue [$d_{\alpha N}(i-1, i)$]. $\beta(i)$ represents the NOE cross peak between ^{1}HN and β ^{1}H in the same residue [$d_{N\beta}(i, i)$]; $\beta(i-1)$ between ^{1}HN and β ^{1}H of the preceding residue [$d_{\beta N}(i-1, i)$]. Connectivities for sequential assignments are represented by lines [$d_{NN}(i-1, i)$] and dashed lines [$d_{\alpha N}(i-1, i)$]. The NOE $d_{\alpha N}(i-3, i)$ cross peaks are indicated by arrows. Assigned amino acids are shown at the bottom.

TABLE I. **Chemical shifts of assigned NMR signals of YCM0-N at neutral pH and 30°C: (A) Mg^{2+}-form and (B) Ca^{2+}-form.**

A

Residue	^{15}N	HN	Hα	Hβ	Other
S1					
S2					
N3					
L4					
T5	117.62	8.83	4.47		γ1.34
E6	124.45	8.98	3.94	2.06	γ2.35, γ' 2.42
E7	123.56	8.61	4.05	2.05	γ2.35
Q8	124.47	7.70	3.74	2.21, 2.30	γ1.38
I9		8.23	3.44	1.84	γ0.96, γ1.11, γ' 1.77, δ0.83
A10	124.96	7.90	4.15	1.52	
E11	123.89	7.80	4.15	2.05, 2.12	γ2.30, γ' 2.45
F12	124.72	8.83	4.92	3.53, 3.62	δ7.07, ε7.18, ζ7.28
K13	125.94	9.23	3.91	1.93	γ1.01, γ' 1.12, δ1.40, ε2.70
E14	123.06	7.90	4.08	2.19	γ2.31, γ' 2.44
A15	125.46	7.88	4.34	1.73	
F16	122.07	8.55	3.66	2.97, 3.30	δ6.62, ε7.23, ζ7.37
A17	121.69	8.26	4.18	1.54	
L18		7.56	3.89	1.41, 1.68	γ1.22, δ0.74, δ' 0.83
F19	118.34	7.19	4.33	2.40, 3.05	δ7.48, ζ7.37
D20	126.09	7.49	5.26	1.95, 2.81	
K21	127.17	7.82	4.00	1.89	γ1.53
D22					
N23					
N24		8.09	4.36	2.71, 3.04	
G25	118.49	10.80	3.80, 4.45		
S26	117.34	7.84	5.80	3.57, 3.71	
I27		9.13		2.12	γ1.81, γ' 0.29, δ0.06
S28	120.81	8.76	4.83	4.01, 4.37	
S29					
S30					
E31					
L32					
A33		8.25	3.85	1.49	
T34	117.94	7.51	3.75	3.98	γ1.03
V35		8.31	3.25		γ0.63, γ' 0.76
M36					
R37	123.19	8.51	3.78	1.97, 2.10	δ2.93
S38	122.65	8.19	4.42	4.17, 4.23	
L39	125.09	7.37	4.57	1.85	γ1.75, δ0.97, δ' 1.13
G40	110.62	7.91	3.84, 4.32		
L41	124.73	7.78	4.59	1.46, 1.59	δ0.83
S42		8.68	4.59		
P43			4.58	2.05, 2.22	
S44	122.39	8.81	4.69	4.05, 4.36	
E45	126.11	8.82	3.93	2.04	γ2.27
A46	124.92	8.30	4.14	1.42	
E47		7.78	4.16	2.29	γ2.45
V48		8.19	3.51	2.15	γ0.96
N49		8.06	4.47	2.80, 2.84	
D50		8.07	4.47	2.72, 2.80	
L51		8.15	4.09	1.89	γ1.40
M52	120.33	8.36	4.10	2.15	γ2.68, ε1.40
N53	116.97	7.95	4.55	2.90, 2.95	δ6.87, δ' 7.76
E54					
I55					
D56					
V57					
D58					
G59	112.51	7.89	3.92		
N60					
H61					
Q62			4.79		
I63	125.18	9.40	4.93	2.00	γ1.04
E64	129.40	8.74	5.33	2.06, 2.47	
F65	127.06	8.79	3.47	2.46, 2.78	δ6.59, ε6.92, ζ7.46
S66	116.97	9.00	3.75	3.89, 3.96	
E67	127.37	6.97	4.17	2.03	γ2.40, γ' 2.53
F68	125.85	8.24	4.07	3.04, 3.21	δ6.97, ε7.48
L69	122.88	8.38	3.31	1.28, 1.31	γ1.04, δ0.77
A70	125.66	7.28	4.01	1.49	
L71	124.11	7.89	3.92	1.66	γ1.48
M72		7.68	4.27	1.24	γ1.47, ε0.09
S73	117.91	8.16	4.10	3.96, 4.01	
R74	122.91	7.36	4.22	1.94, 1.82	γ1.69
Q75		7.88	4.16	2.03, 2.20	γ2.42, ε7.23
L76	124.57	7.62	4.36	1.70	γ1.78, δ0.95, δ' 0.91
K77	130.28	7.51	4.10	1.78, 1.84	γ1.48, ε3.05

B

Residue	^{15}N	HN	Hα	Hβ	Other
S1					
S2					
N3					
L4					
T5	118.07	8.79	4.50	2.37	γ1.36
E6	124.76	9.04	4.00	2.07	γ2.36, γ' 2.40
E7	123.99	8.73	4.07	2.06, 1.93	γ2.28, γ' 2.36
Q8	124.76	7.76	3.86	2.28	γ2.35
I9	123.99	8.36	3.17	1.98	γ1.13, δ0.90
A10	125.79	8.01	4.12	1.54	
E11	123.99	7.78	4.14	2.04, 1.94	γ2.42
F12	124.76	8.60	5.09	3.52	δ7.22, ε7.28, ζ7.58
K13	128.11	9.20	4.02	1.92	γ1.86, δ1.26
E14	124.50	7.74	4.13	1.90	γ2.17, γ' 2.35
A15	126.82	7.79	4.13	1.92	
F16	122.96	8.79			δ6.63, ε7.05, ζ7.38
A17					
L18					
F19					
D20	120.64	7.73	4.53	2.58, 2.91	
K21	129.91	7.54	4.03	1.94	γ1.59
D22	118.58	8.04	4.61	3.09, 2.56	
N23	119.61	7.98	4.35	3.09, 2.75	δ6.70, δ' 7.49
N24	121.67	8.45	4.86	2.53, 3.31	δ7.05, δ' 7.83
G25	**119.35**	**10.81**	**4.39, 3.70**		
S26	116.78	7.75	5.18	3.83, 3.87	
I27	131.71	9.78	5.18	1.98	γ0.93, δ0.31
S28	129.39	9.04	4.74	4.14	
S29	120.64	9.34	4.75	3.98	
S30	120.64	8.13	4.75	3.94, 4.32	
E31	128.11	7.60	4.30	2.22	γ2.49
L32	127.33	9.06		2.08	γ1.38, δ0.92
A33					
T34	125.27	7.69	4.55	1.65	γ2.69
V35	119.61	7.77	4.03	1.93	γ1.03, γ' 1.25
M36	123.99	7.37	3.93	1.98	
R37	130.94	7.74	4.18	1.85, 1.75	γ1.42, δ3.04
S38					
L39	123.47	8.22	4.76	1.96	
G40	123.73	8.13	4.42, 4.26		
L41	124.50	7.63	4.49	1.86	γ1.50, δ0.82
S42	118.84	8.70	4.76	3.74, 3.86	
P43					
S44	126.05	8.90	4.75	4.59, 4.36	
E45	126.05	8.90	3.93	2.06	γ2.34
A46	125.27	8.32	4.14	1.42	

TABLE I. (Continued)

Residue	^{15}N	HN	Hα	Hβ	Other
E47	122.44	7.61	4.07	1.94	γ2.35
V48	**126.05**	**8.15**	**3.53**	**2.20**	**γ1.04**
N49	122.44	7.95	4.36	2.86	
D50	124.50	8.39	4.46	2.70	
L51	126.82	7.73	4.25	1.92	γ1.57, δ0.92
M52	122.96	8.59	3.99	2.26	γ2.37, ϵ1.94
N53	118.58	8.00	4.50	2.92, 2.87	
E54	122.44	7.66	4.14	2.20, 2.14	γ2.40
I55	128.36	7.70	4.54		
D56	125.27	8.30	4.74	2.92, 2.50	
V57	129.91	8.12	3.96	2.23	γ1.11, γ' 1.10
D58	120.90	8.27	4.64	2.98, 2.64	
G59	112.66	7.56	3.89, 3.76		
N60	122.70	8.14	4.54	3.19, 2.63	
H61	122.44	10.49	3.96	3.48	ϵ8.55, δ7.24
Q62	117.29	7.52		1.71	γ2.13, γ' 2.27
I63	129.91	9.52	5.31	2.25	γ1.16, δ0.86
E64	133.77	8.72	4.89	2.33, 2.13	γ2.59
F65	128.36	9.39	4.77		δ6.76, ϵ7.26, ζ7.40
S66	116.52	8.95	3.92	3.89, 3.74	
E67	127.33	6.86	4.32	2.29	γ2.75, γ' 2.56
F68	127.33	8.47	3.98	3.43	
L69	122.96	8.35	3.37		δ0.07
A70	126.05	7.15	4.01	1.53	
L71	122.44	7.43	3.97	1.53	γ1.46, δ0.83, δ' 0.57
M72					
S73	118.07	7.93	4.25	4.00, 3.88	
R74	124.76	7.32	4.24	1.91, 1.82	γ1.70
Q75	121.67	7.83	4.31	2.25, 2.03	γ2.42, γ' 2.34
L76					
K77					

The region from Ser66 to Gln75 is identified as the fourth helix, D-helix. The CSI values and the $d_{N\alpha}/d_{\alpha N}$ ratios of Leu76 and Lys77 suggest that these two residues are in a disordered conformation.

The $d_{N\alpha}/d_{\alpha N}$ ratios of Ser26, Ile27, and Ser28 are smaller than unity. Ser26 and Ile27 show negative CSI values. Ile63 and Glu64 have negative CSI values and the $d_{N\alpha}/d_{\alpha N}$ ratios are smaller than unity. The results and the comparison with vertebrate CaM suggest that Ser26-Ser28 and Gln62-Glu64 are in a β-strand. Figure 3A shows the schematic representation of NOE observed for the β-strands. NOEs between Ser26 and Glu64, and between Ile27 and Ile63 are found. These NOEs suggest that the β-strands are hydrogen-bonded to each other. This region is identified as a short antiparallel β-sheet. An expected NOE cross peak between Ser28 α^1H and Gln62 α^1H is difficult to observe in the 2D-NOESY spectra because of the large water peak.

The present results indicate that YCM0-N in the Mg^{2+}-form has four helices (A, B, C, and D) and an antiparallel β-sheet.

Secondary Structure of YCM0-N in the Ca^{2+}-Form—Figure 2B shows the data for determination of the secondary structure of YCM0-N in the Ca^{2+}-form. The first three residues in the N-terminus (Ser1 to Asn3) are not assignable. The characteristic NOE $d_{\alpha N}(i-3, i)$ connectivities are found from Glu6 to Phe16; the residues constitute the A-helix. The NOE $d_{\alpha N}$ (5, 8) is not observed in the 2D-NOESY and the ^{15}N-edited 3D-NOESY spectra, although the NOE $d_{\alpha N}$ (4, 7) is observed. The CSI values of Leu4 and Thr5 are negative and the $d_{N\alpha}/d_{\alpha N}$ ratios are smaller than unity. Thus, the N-terminal end of A-helix is identified as Glu6. Because Ala17, Leu18, and Phe19 are not assigned, the C-terminal end of A-helix is not determined. A-helix spans from Glu6 to at least Phe16. Phe12 of YCM0-N in the Ca^{2+}-form shows negative CSI, as in the Mg^{2+}-form.

Figure 4 shows strips of 2D-NOESY slice planes at different ^{15}N chemical shifts of the ^{15}N-edited 3D-NOESY spectrum for the Ca^{2+}-form YCM0-N. This figure shows the amide signals of the residues in the B-helix region and their NOE peaks. The NOE $d_{\alpha N}(i-3, i)$ peak is not observed. NMR data at different NOE mixing-times, temperatures, pH values, and concentrations do not show any characteristic NOE $d_{\alpha N}(i-3, i)$ connectivity for residues in the B-helix region, suggesting no formation of B-helix on the NMR time scale.

YCM0-N in the Mg^{2+}-form has B-helix as described in the previous section. Vertebrate CaM in the Ca^{2+}-form has B-helix as reported previously (*2-4*). Therefore, the fact that B-helix is not formed is a novel finding for yCaM in the Ca^{2+}-form.

The CSI values of Thr34-Arg37 are positive and the $d_{N\alpha}/d_{\alpha N}$ ratios are greater than unity, suggesting a possibility of nascent helical conformation. This is supported by evidence that NOE cross peaks between the side-chains of Thr34 and of Arg37 are observed (data not shown).

The C-helix is well defined for residues from Glu45 to Glu54. The characteristic NOE $d_{\alpha N}(i-3, i)$ connectivities are observed from Ser66 to Arg74, except for unassigned Met72. For these residues, the CSI values are positive and the $d_{N\alpha}/d_{\alpha N}$ ratios are mostly greater than unity. This region is, therefore, identified as D-helix. Leu76 and Lys77 are not assigned.

Negative CSI values and $d_{N\alpha}/d_{\alpha N}$ ratios less than unity are observed for Ser26 to Ser28 and for Gln62 to Glu64, suggesting that these residues form β-strands. Some other NOEs of β-strand regions are also observed, as shown in Fig. 3B. The NOEs between Ser26 and Glu64 and between Ile27 and Ile63 indicate that the β-strands are connected with each other. The results indicate that the two β-strands comprise a short antiparallel β-sheet. The NOE cross peak between α^1H's of Ser28 and Gln62 is not identified because the expected position of the cross peak is under the water peak. The presence of β-sheet for Ca^{2+}-saturated yCaM has been reported by Klevit and co-workers (*23*).

Thus, three helices A, B, and D and an antiparallel β-sheet are identified for YCM0-N in the Ca^{2+}-form.

Ca^{2+}-Titration by HSQC—We observed the sensitivity enhanced 2D-(^{1}H,^{15}N)-PFG-HSQC spectra at various Ca^{2+} concentrations. A number of signals of YCM0-N in the Mg^{2+}-form (Fig. 5A) decrease in intensity with increasing Ca^{2+} concentration. The decrease continues until the $[Ca^{2+}]/[YCM0\text{-}N]$ ratio reaches about 2. At the expense of the signals of the Mg^{2+}-form, signals of the Ca^{2+}-form appear at new positions, as shown in Fig. 5B, and increase in intensity upon Ca^{2+}-addition. The increase also continues until the $[Ca^{2+}]/[YCM0\text{-}N]$ ratio reaches about 2. The spectral change with Ca^{2+} addition reflects the equilibrium between Mg^{2+}-form and Ca^{2+}-form.

Figure 6 shows the relative change of signal intensity plotted against the $[Ca^{2+}]/[YCM0\text{-}N]$ ratio. The relative change is estimated as the ratio of peak heights in the HSQC spectra. The change in intensity occurs until the

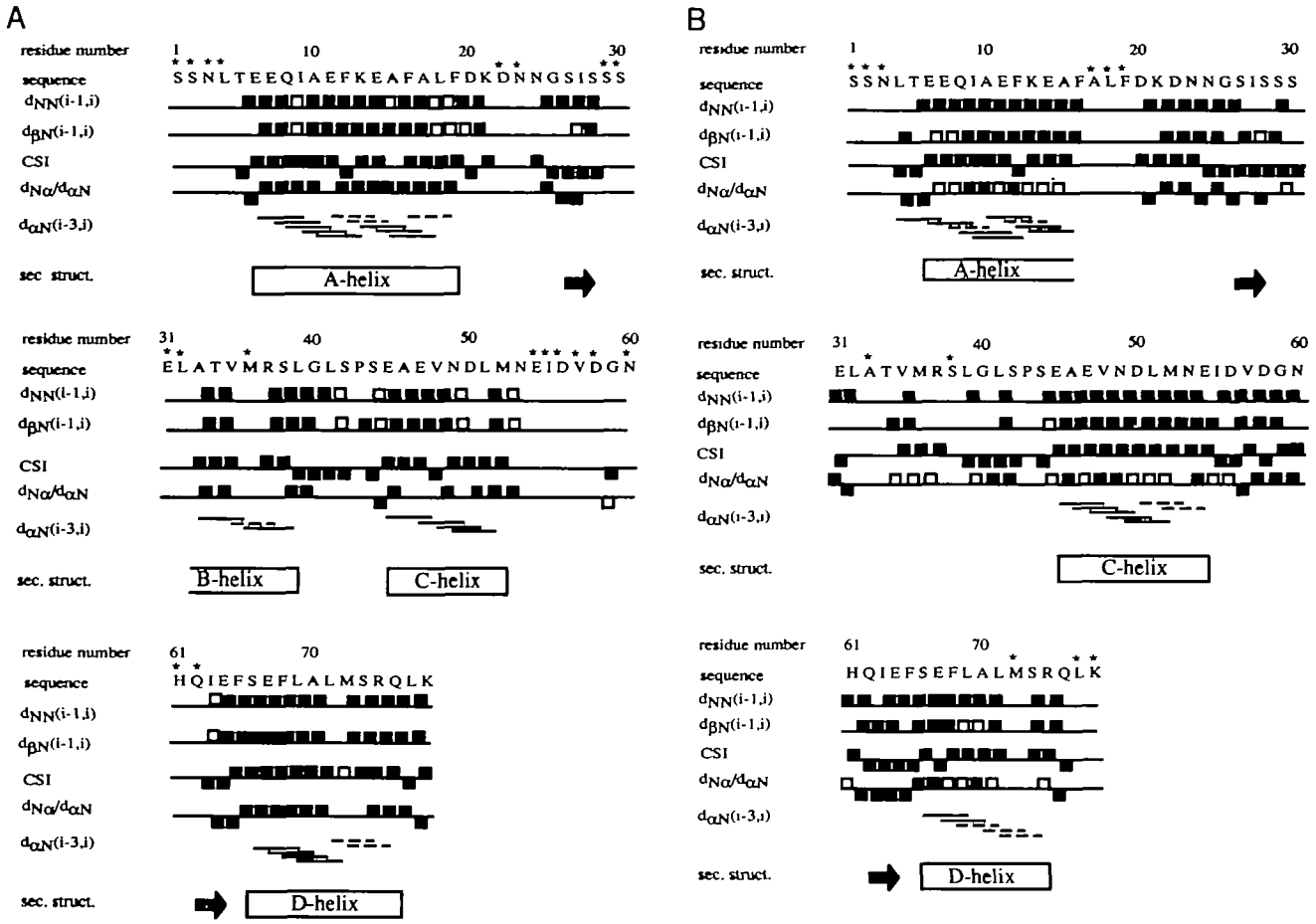

Fig. 2. **Schematic representation of secondary structure determination for YCM0-N in the presence of Mg^{2+} (A) and Ca^{2+} (B).** Experimental conditions are described in "MATERIALS AND METHODS." Filled squares represent observed NOE $d_{NN}(i-1, i)$ (NOE connectivity between two amide protons of residues $i-1$ and i), and NOE $d_{\beta N}(i-1, i)$ (NOE connectivity between β proton of residue $i-1$ and amide proton of residue i). CSI (the chemical-shift index for α^1H) is represented by upward and downward filled squares, which indicate positive and negative values, respectively. $d_{N\alpha}/d_{\alpha N}$ [the NOE intensity ratio between $d_{N\alpha}(i, i)$ and $d_{\alpha N}(i-1, i)$] is also represented by upward and downward filled squares, which indicate $d_{N\alpha}/d_{\alpha N}>1$ and $d_{N\alpha}/d_{\alpha N}<1$, respectively. $d_{\alpha N}(i-3, i)$ (NOE connectivity between α^1H_{i-3} and ^1HN_i) is represented by lines. Broken lines and open squares indicate uncertain results due to signal overlapping or weak intensity close to the noise level. Residues marked with * are not assigned. Boxes with the helix name represent determined helix regions. The box with one side open represents a helix of which the edge is not determined. β-Strand regions are represented by arrows.

$[Ca^{2+}]/[YCM0\text{-}N]$ ratio reaches about 2, indicating that YCM0-N binds two Ca^{2+} ions. The results support the previous 1D ^{1}H-NMR findings (*23*).

The observed spectral changes induced by Ca^{2+}-binding are difficult to group into a small number of types. There is no apparent relationship between the spectral change and amino acid type and/or location.

The magnitude of chemical shift difference between the two forms, $|\delta Ca^{2+} - \delta Mg^{2+}|$, was estimated for ^{15}N, ^{1}HN, and α^1H resonances of each residue. These values were normalized based on the maximum of each resonance. The three normalized data of ^{15}N, ^{1}HN, and α^1H were averaged for each residue. The results are shown in Fig. 7. The chemical shift differences are greater in the two Ca^{2+}-binding loops than in the helix regions. The region corresponding to B-helix shows greater chemical shift difference than the other helix parts. The results indicate that the B-helix region is greatly modified by Ca^{2+}-binding. This is in accord with the above results indicating that B-helix is not formed in the Ca^{2+}-form.

DISCUSSION

Location of Secondary Structure Elements—Helix and β-sheet regions of YCM0-N in the Mg^{2+}- and Ca^{2+}-forms together with the data for the N-domain of Ca^{2+}-loaded *Drosophila* CaM (*47*) are summarized in Table II. The location of secondary structure elements of YCM0-N are mostly the same in both forms, except for the unformed B-helix in the Ca^{2+}-form. The Ca^{2+}-induced conformational change in YCM0-N involves the destruction of B-helix and/or a change of orientation of the secondary structure elements.

The location of secondary structure elements of YCM0-N in the Ca^{2+}-form is mostly the same as that of the N-domain of Ca^{2+}-loaded *Drosophila* CaM, except for unformed B-helix. The results are noteworthy, because the homology in amino acid sequence between the two CaMs is only 60%.

β-Sheet—The amide resonances of Ile27 and Ile63 comprising the β-sheet appear at lower fields in the Ca^{2+}-form

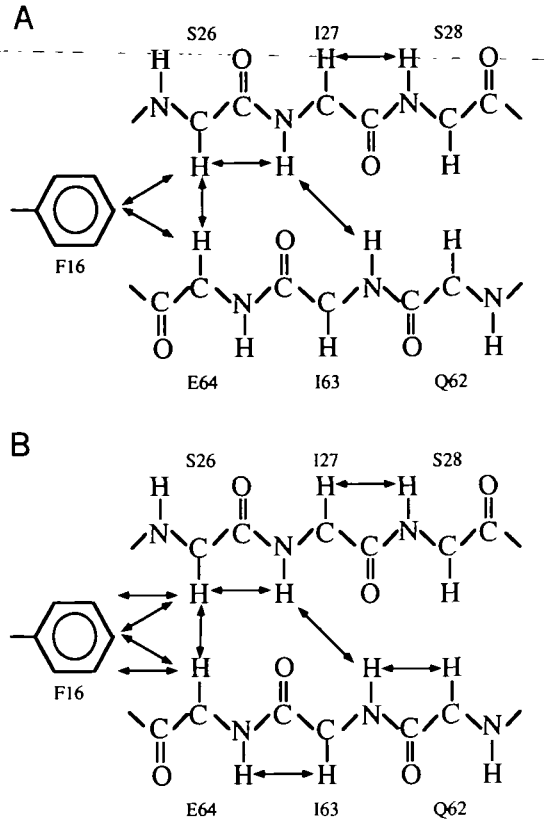

Fig. 3. **Schematic representation of the β-sheet region for YCM0-N in the presence of Mg^{2+} (A) and Ca^{2+} (B).** The phenyl ring of the Phe16 residue that is close to the β-sheet is included in the figure. Amino acid residues that participate in forming the β-sheet are shown. Identified NOE connectivities are depicted by double-headed arrows.

than in the Mg^{2+}-form (shown in Table I and Fig. 5). Since low-field shift of amide proton resonance is indicative of stronger hydrogen-bonding (*48*), Ile27 and Ile63 form stronger hydrogen-bonding in the Ca^{2+}-form than in the Mg^{2+}-form. This implies that the β-sheet of the Ca^{2+}-form is more stable than that of the Mg^{2+}-form.

Hydrophobic Core—Figure 8 shows an NOE contact map of YCM0-N in the Mg^{2+}- and Ca^{2+}-forms. NOEs between hydrophobic residues of Ile9, Phe12, Phe16, Phe19, Ile27, Phe65, and Phe68 are observed in both forms, indicating that these residues are located within 5 Å of each other. Side-chains of these residues in YCM0-N form a hydrophobic core, as in vertebrate CaM (*2–9*). yCaM binds a hydrophobic molecule in a Ca^{2+}-dependent manner (*22*). The hydrophobic core in the N-domain of yCaM is suggested to be one of the binding sites for targets as in the case of CaM.

B-Helix—The B-helix of site I in YCM0-N was identified in the Mg^{2+}-form, but not in the Ca^{2+}-form. In HSQC spectra of the Ca^{2+}-form YCM0-N, the amide signals of Ser29 and Leu32 at the N-terminus of the B-helix region are weak and signals of Ser30 and Glu31 are not observed as shown in Fig. 5B. These results suggest that a conformational exchange occurs for these residues of Ca^{2+}-form YCM0-N. This is in accord with the finding that the B-helix is not formed on the NMR time scale for Ca^{2+}-form YCM0-N. The fact that the B-helix is destroyed by Ca^{2+}-binding seems to support the previous CD result that the helix content of intact yCaM is decreased by Ca^{2+}-binding (*18, 22*).

The difference of amino acid residues in the region of the B-helix between yCaM and vertebrate CaM occurs only in the N-terminal region. Thr29 and Lys30 in the N-terminal region of the B-helix for vertebrate CaM are replaced with Ser29 and Ser30 for yCaM, respectively. The replacement causes an alteration in the electrostatic environment.

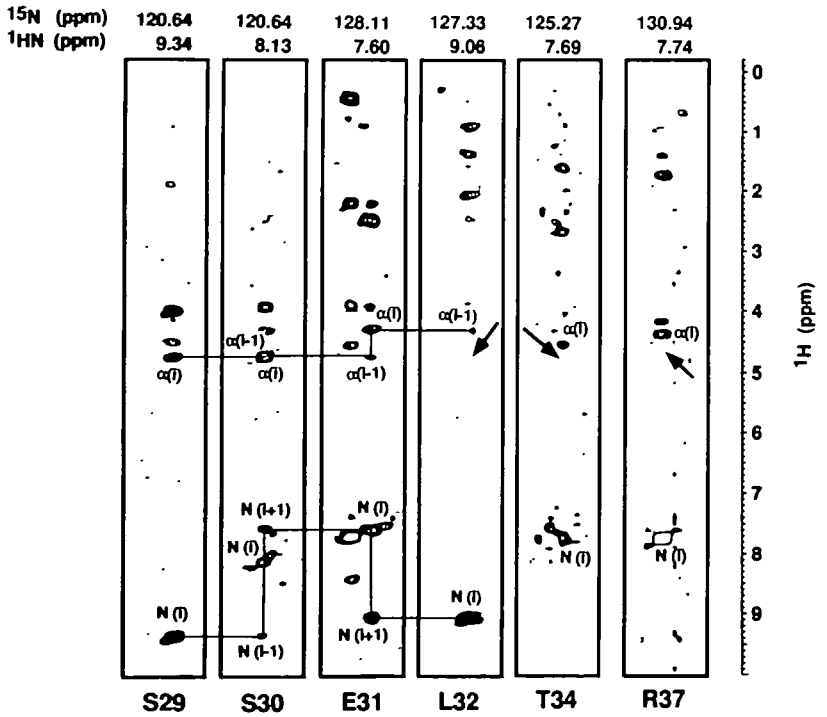

Fig. 4. **Strips of 2D-NOESY slice planes for resonances corresponding to the B-helix region at different ^{15}N chemical shifts in ^{15}N-edited 3D-NOESY spectra of Ca^{2+}-form YCM0-N (500 MHz, mixing time 150 ms, 30°C).** Sample conditions are described in "MATERIALS AND METHODS." The ^{15}N chemical shift of the slice plane and the ^{1}HN chemical shift of the strip are shown at the top of the figure. Symbols are the same as in Fig. 1. Assigned amino acids are shown at the bottom in the figure. The NOE $d_{\alpha N}(i-3, i)$ cross peaks do not appear at the expected positions indicated by arrows. Signals of Ala33 and Ser38 are not identified (see the caption of Fig. 2). Sequential connectivities are represented by lines.

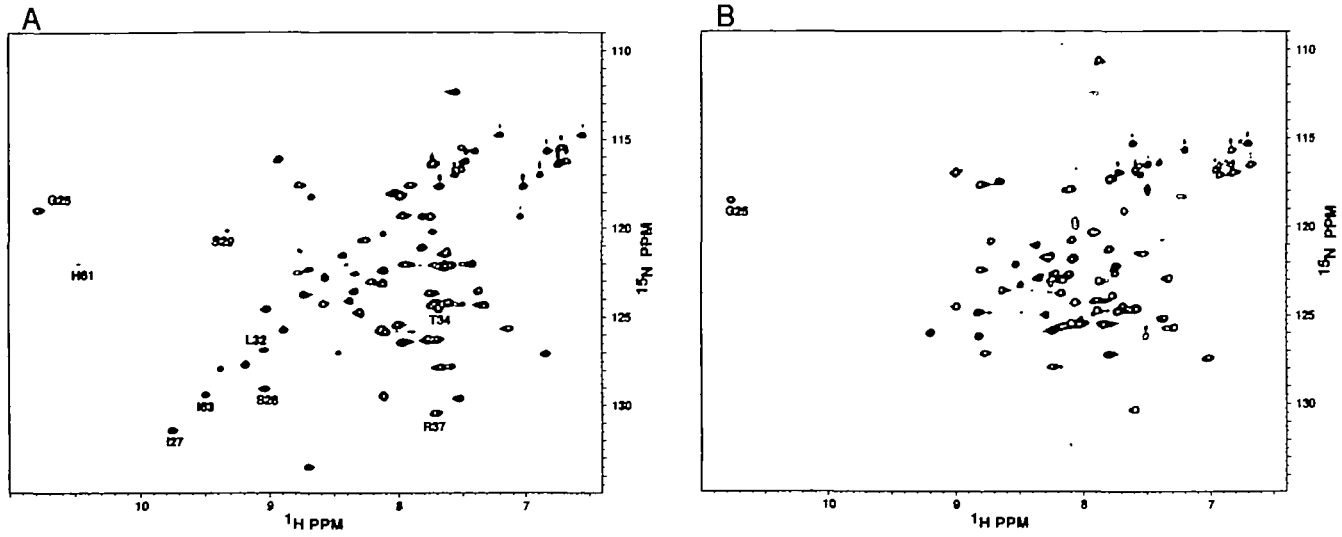

Fig. 5. **Sensitivity enhanced 2D-(^{1}H, ^{15}N)-PFG-HSQC spectra of YCM0-N at 30°C observed at a ^{1}H frequency of 500 MHz.** Conditions: (A) [YCM0-N] = 3 mM, [KCl] = 50 mM, [Mg^{2+}] = 300 mM, and pH = 6.5-7.0; (B) [YCM0-N] = 3 mM, [KCl] = 50 mM, [Mg^{2+}] = 300 mM, [Ca^{2+}] = 9.0 mM, and pH = 6.5-7.0. To avoid congestion, only a few signals are labeled with the amino acid residue number.

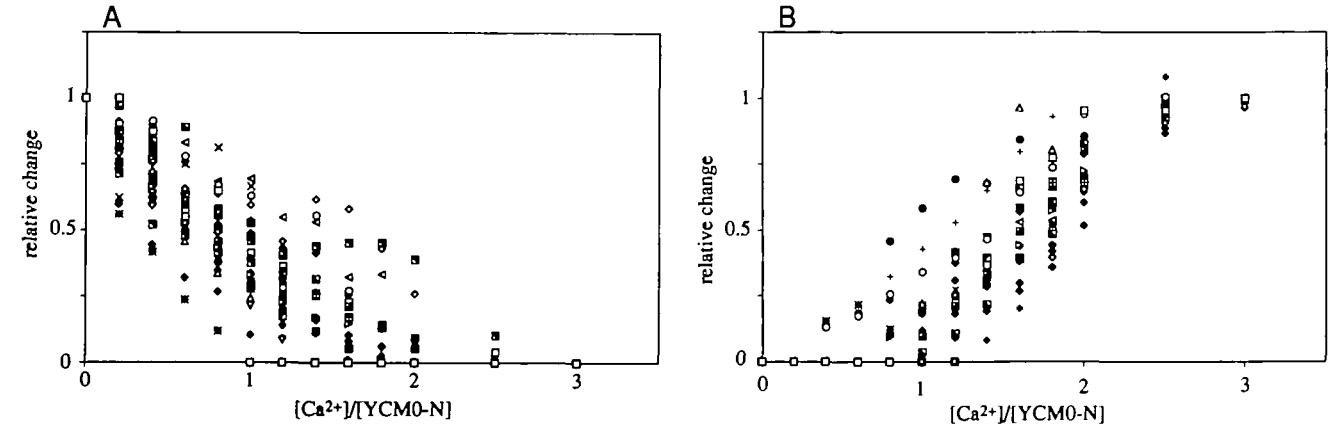

Fig. 6. **Plot of relative change in signal intensity of sensitivity enhanced 2D-(^{1}H, ^{15}N)-PFG-HSQC spectra against the [Ca^{2+}]/[YCM0-N] ratio.** (A) Mg^{2+}-form (■, Glu6; ◇, Glu7; ○, Gln8; △, Phe12; ▲, Lys13; ⊕, Ala15; ⊕, Phe16; ▽, Asp20; ◪, Lys21; ◆, Ser26; ✱, Ser28; ▷, Arg37; ◩, Leu39; ◐, Leu41; ×, Ser44; ◁, Gly59; ◙, Ser66; ◆, Glu67; +, Phe68; ⊕, Leu69; ◙, Ala70; ◆, Leu71; ⧖, Ser73; ▯, Arg74; and ◇, Ser77), and (B) Ca^{2+}-form (▯, Glu6; ◇, Phe12; ○, Lys13; △, Ala15; ▯, Lys21; ⊕, Asp22; ⊕, Asn23; ▽, Asn24; ◪, Ser26; ◆, Ile27; ✱, Arg37; ▷, Glu47; ◩, Leu51; ◆, Asn53; ×, Val57; ◁, Asp58; ◙, Ile63; ◆, Glu64; +, Glu67; ⊕, Phe68; ◙, Ala70; and ◆, Leu71). The relative change is estimated as relative peak height.

Mutagenesis studies showed that the helix stability depends on the amino acid type of the N-terminal end residues of the helix (*49-51*). The sequence of Ser29-Ser30 may cause differences in the conformation and stability of the N-terminal side of the B-helix region between YCM0-N and vertebrate CaM.

Signals of Thr34 and Arg37 are clearly observed in the HSQC spectra of Ca^{2+}-form YCM0-N (Fig. 5B). The nascent helical conformation in Thr34-Arg37 suggests that the influence of amino acid replacement in the N-terminal side of the B-helix is small in the C-terminal side of the helix.

It is reported that for Ca^{2+}-saturated vertebrate CaM not only the solvent exposed hydrophobic core, but also the side chains of Leu32, Val35, and Met36 in B-helix interact with the target (*52-55*). It is known that yCaM activates vertebrate targets, such as MLCK and PDE, less than vertebrate CaM does. The poor activity of yCaM for vertebrate targets may be related to be the instability of the B-helix.

Ser29-Leu32 are not assigned in the Mg^{2+}-form. This region is probably disordered. Val35 and Met36 in the B-helix region are close to the hydrophobic core in the Mg^{2+}-form, as shown in Fig. 8. The hydrophobic interaction is presumably responsible for the stability of B-helix in the Mg^{2+}-form.

Ca^{2+}-Binding Site I—It has been believed that the high affinity for Ca^{2+} is caused by the helix-loop-helix structure. This leads to the question of whether site I of YCM0-N serves as a Ca^{2+}-binding site, because the second helix (B-helix) of helix-loop-helix structure is not formed, as mentioned above. However, Ca^{2+}-titration monitored by

TABLE II. **Summary of helix and β-sheet regions of YCM0-N (N-terminal half domain of yeast calmodulin) in the presence of Mg^{2+} and Ca^{2+} in comparison with the Ca^{2+}-loaded N-domain of *Drosophila* CaM (calmodulin) (*1, 47*).** Plus signs (+) before and after residue number indicate the possibility that the helix extends before and after the residue, respectively.

	YCM0-N (Mg^{2+})	YCM0-N (Ca^{2+})	N-domain of Ca^{2+}-loaded *Drosophila* CaM
A-helix	6-19	6-15+	6-18
B-helix	+33-39	non	29-39
C-helix	45-52	45-54	45-55
D-helix	66-75	66-74	65-76
β-sheet	26-28, 62-64	26-28, 62-64	26-28, 62-64

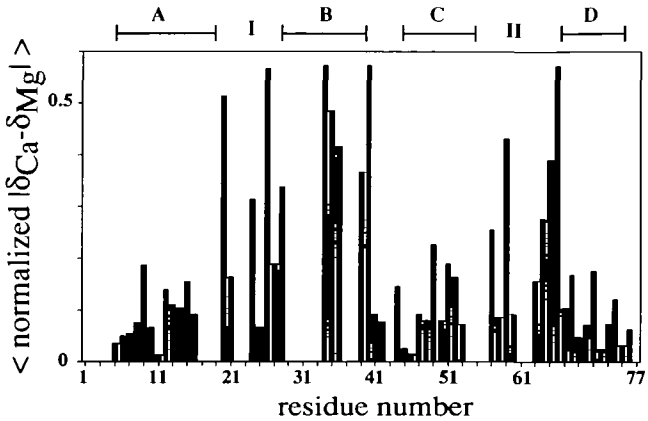

Fig. 7. **Magnitude of chemical shift difference as a function of residue number.** The value for each residue is an average of the normalized chemical shift differences of α^1H, ^{1}HN, and ^{15}N resonances. Residues which do not have a bar are not assigned in the Mg^{2+} and/or Ca^{2+}-form.

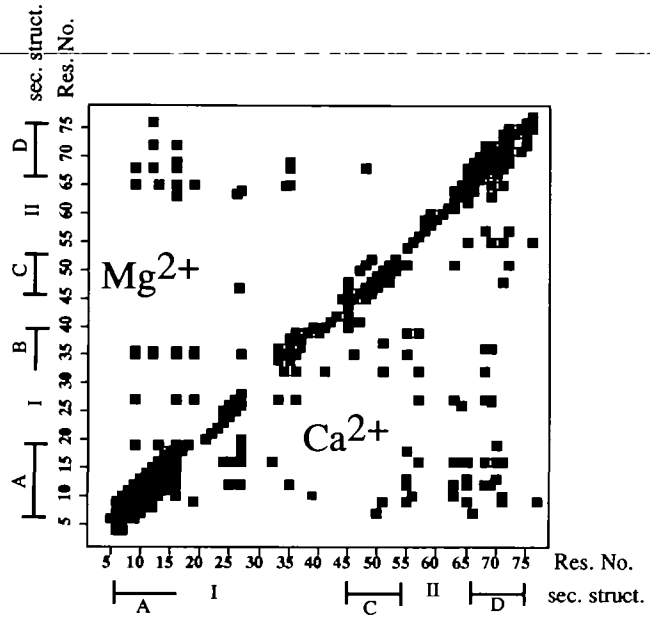

Fig. 8. **NOE contact map of YCM0-N in the Mg^{2+}- and Ca^{2+}-forms.** The upper left triangle indicates the results for the Mg^{2+}-form, and the lower right triangle, for the Ca^{2+}-form. Filled boxes indicate NOE connectivity observed in 2D-NOESY or ^{15}N-edited 3D-NOESY spectra (mixing time = 150 ms). NOE of side-chain protons as well as main-chain protons is taken into account.

2D-HSQC indicates that YCM0-N does bind two Ca^{2+} ions, *i.e.*, site I of the imperfect helix-loop-helix binds a Ca^{2+} ion. The Ca^{2+}-binding constant of yCaM is reported to be of the magnitude of 10^{-6} M (*23*), *i.e.*, a normal Ca^{2+}-affinity of EF-hand structure.

The ligands in site I of yCaM for Ca^{2+}-binding are expected to be Asp20, Asp22, Asn24, Ser26, Ser28, and Glu31. The first three ligand residues which comprise the Asx turn (*5, 56*) are well conserved. Glu at the end of the loop is also conserved. In addition, the β-sheet formed by Ser26, Ile27, and Ser28 is conserved. The conservative conformation of Asx turn and β-sheet probably contributes to the Ca^{2+}-affinity of site I in yCaM.

D-Helix—Figure 8 suggests that the D-helix is close to the A-helix in both forms, suggesting that these two helices are paired with each other. Such paired helices connecting two EF-hand sites are reported for TnC and vertebrate CaM (*7, 57*).

Ca^{2+}-Titration by HSQC—Recently, Sykes and co-workers reported similar results of Ca^{2+}-titration monitored by 2D-HMQC for the regulatory domain of troponin C (NTnC), which has two Ca^{2+}-binding sites (*58*). They showed that there are three types of Ca^{2+}-induced spectral change, and that the different types appear randomly along the amino acid sequence.

However, the present results do not indicate that the Ca^{2+}-induced spectral change of YCM0-N can be classified into two or three types (*59*). It seems that the local conformational change and its dynamics occur differently from residue to residue, presumably through multiple intermediates. Further study is needed to explain the Ca^{2+}-titration results.

At present, the three-dimensional structure analysis is obstructed by an insufficient number of NOE constraints. Efforts to improve the quality of NMR NOE data (including ^{13}C labeling) are in progress.

We are grateful to Professor F. Morita of Hokkaido University for helping us to obtain samples. We thank Frank Dellagrio and Daniel S. Garett of NIH for providing their NMR data processing programs. We also thank the NMR application laboratory of JEOL Ltd. for valuable advice on NMR measurements.

REFERENCES

1. Crivici, A. and Ikura, M. (1995) Molecular and structural basis of target recognition by calmodulin. *Annu. Rev. Biomol. Struct.* **24**, 85-116
2. Babu, Y.S., Bugg, C.E., and Cook, W.J. (1988) Structure of calmodulin refined at 2.2 Å resolution. *J. Mol. Biol.* **204**, 191-204
3. Chattopadhyaya, R., Meader, W.E., Means, A.R., and Quiocho, F.A. (1992) Calmodulin structure refined at 1.7 Å resolution. *J. Mol. Biol.* **228**, 1177-1185
4. Rao, S.T., Wu, S., Satyshur, K.A., Ling, K.Y., Kung, C., and Sundralingam, M. (1993) Structure of Paramecium teraurelia calmodulin at 1.8 Å resolution. *Protein Sci.* **2**, 436-444
5. McPhalen, C.A., Strynadka, N.C.J., and James, M.N.G. (1991) Calcium-binding sites in proteins: A structural perspective. *Adv. Protein Chem.* **42**, 77-144
6. Finn, B.E., Drakenberg, T., and Forsén, S. (1993) The structure of apo-calmodulin: A ^{1}H-NMR examination of the carboxy-teminal domain. *FEBS Lett.* **336**, 368-374
7. Zhang, M., Tanaka, T., and Ikura, M. (1995) Calcium-induced

conformational transition revealed by the solution structure of apo calmodulin. *Nature Struct. Biol.* **2**, 758-767
8. Kuboniwa, H., Tjandra, N., Grzesiek, S., Ren, H., Klee, C.B., and Bax, A. (1995) Solution structure of calcium-free calmodulin. *Nature Struct. Biol.* **2**, 768-776
9. Finn, B.E., Evenäs, J., Drakenberg, T., Waltho, J.P., Thulin, E., and Forsén, S. (1995) Calcuim-induced structural changes and autonomy in calmodulin. *Nature Struct. Biol.* **2**, 777-783
10. Drabiowski, W., Brzeska, H., and Venyaminov, S.Y. (1982) Tryptic fragment of calmodulin: Ca^{2+}- and Mg^{2+}-induced conformational changes. *J. Biol. Chem.* **257**, 11584-11590
11. Tsai, M.D., Drakenberg, T., Thulin, E., and Forsen, S. (1987) Is the binding magnesium (II) to calmodulin significant?: An investigation by magnesium-25 nuclear magnetic resonance. *Biochemistry* **26**, 3635-3643
12. Ogawa, Y. and Tanokura, M. (1984) Calcium binding to calmodulin: Effects of ionic strength, Mg^{2+}, pH, and temperature. *J. Biochem.* **95**, 19-28
13. Milos, M., Schaer, J., Comte, M., and Cox, J.A. (1986) Calcium-proton and calcium-magnesium antagonism in calmodulin: Microcalorimetric and potentiometric analyses. *Biochemistry* **25**, 6279-6287
14. Ohki, S., Yazawa, M., Yagi, K., and Hikichi, K. (1991) Mastoparan binding induces Ca^{2+}-transfer between two globular domain of calmodulin: A ^{1}H NMR study. *J. Biochem.* **110**, 737-742
15. Ohki, S., Iwamoto, U., Aimoto, S., Yazawa, M., and Hikichi, K. (1993) Mg^{2+} inhibits formation of $4Ca^{2+}$-calmodulin-enzyme complex at lower Ca^{2+} concentration. *J. Biol. Chem.* **268**, 12388-12392
16. Luan, Y., Matsuura, I., Yazawa, M., and Yagi, K. (1987) Yeast calmodulin: Structural and functional differences compared with vertebrate calmodulin. *J. Biochem.* **102**, 1531-1537
17. Cohen, P. and Clee, C.B. (1988) *Calmodulin*, pp. 1-15, Elsevier, New York
18. Matsuura, I., Ishihara, K., Nakai, Y., Yazawa, M., Toda, H., and Yagi, K. (1991) A site-directed mutagenesis study of yeast calmodulin. *J. Biochem.* **109**, 190-197
19. Matsuura, I., Ishihara, K., Nakai, Y., Yazawa, M., Toda, H., and Yagi, K. (1993) Mutagenesis of the fourth calcium-binding domain of yeast calmodulin. *J. Biol. Chem.* **268**, 13267-13273
20. Brockhoff, S.E. and Davis, T.N. (1992) Calmodulin concentrates at regions of cell growth in *Saccharomyces cerevisiae*. *J. Cell. Biol.* **118**, 619-629
21. Davis, T.N., Urdea, M.S., Masiarz, F.R., and Thorner, J. (1986) Isolation of the yeast calmodulin gene: Calmodulin is an essential protein. *Cell* **47**, 423-431
22. Ohya, Y., Uno, I., Ishikawa, T., and Anraku, Y. (1987) Purification and biochemical properties of calmodulin from *Saccharomyces cerevisiae*. *Eur. J. Biochem.* **168**, 13-19
23. Starovasnik, M.A., Davis, T.N., and Klevit, R.E. (1993) Similarities and differences between yeast and vertebrate calmodulin: An examination of the calcium-binding structural properties of calmodulin from the yeast *Saccharomyces cerevisiae*. *Biochemistry* **32**, 3261-3270
24. Kay, L.E., Keifer, P., and Saarinen, T. (1992) Pure absorption gradient enhanced heteronuclear single quantum correlation spectroscopy with improved sensitivity. *J. Am. Chem. Soc.* **114**, 10663-10665
25. Schleif, R.F. and Wensink, P.C. (1981) *Practical Methods in Molecular Biology* p. 197, Springer-Verlag, New York
26. Yazawa, M., Sakuma, M., and Yagi, K. (1980) Calmodulin from muscles of marine invertebrates, scallop and sea anemone: Comparison with calmodulins from rabbit skeletal muscle and pig brain. *J. Biochem.* **87**, 1313-1320
27. Rance, M., Sørensen, O.W., Bodenhausen, G., Wagner, G., Ernst, R.R., and Wüthrich, K. (1983) Improved spectral resolution in COSY ^{1}H NMR spectra of proteins via double quantum filtering. *Biophys. Biochem. Res. Commun.* **117**, 479-485
28. Jeener, J., Meier, B.H., Bachmann, P., and Ernst, R.R. (1979) Investigation of exchange process by two dimensional NMR spectroscopy. *J. Chem. Phys.* **71**, 4546-4553
29. Macura, S. and Ernst, R.R. (1980) Elucidation of cross relaxation in liquids by two-dimensional NMR spectroscopy. *Mol. Phys.* **41**, 95-117
30. Braunchweiler, L. and Ernst, R.R. (1983) Coherence transfer by isotopic mixing: Application to proton correlation spectroscopy. *J. Magn. Reson.* **53**, 521-528
31. Davis, D.G. and Bax, A. (1985) Assignment of complex ^{1}H NMR spectra via two-dimensional homonuclear Hartmann-Harn spectroscopy. *J. Am. Chem. Soc.* **107**, 2820-2821
32. Morris, G.A. and Freeman, R. (1978) Selective excitation in fourier transform nuclear magnetic resonance. *J. Magn. Reson.* **29**, 433-470
33. Plateau, P. and Guéron, M. (1982) Exchangeable proton NMR without base-line distortion, using new strong-pulse sequence. *J. Am. Chem. Soc.* **104**, 7310-7311
34. Stonehouse, J., Shaw, G.L., and Keeler, J. (1994) Improving solvent suppression in jump-return NOESY experiments. *J. Biomol. NMR* **4**, 799-805
35. Takegoshi, K., Tsuda, S., and Hikichi, K. (1990) Practical implementation of the self-refocused 1331 solvent-suppression sequence. *J. Magn. Reson.* **89**, 399-405
36. Kay, L.E., Marion, D., and Bax, A. (1989) Practical aspects of 3D heteronuclear NMR of proteins. *J. Magn. Reson.* **84**, 72-84
37. Marion, D., Driscoll, P.C., Kay, L.E., Wingfield, P.T., Bax, A., Gronenborn, A.M., and Clore, G.M. (1989) Overcoming the overlap problem in the assignment of ^{1}H NMR spectra of larger proteins by use of three-dimensional heteronuclear ^{1}H-^{15}N Hartmann-Hahn-multiple quantum coherence spectroscopy: Application to interleukin 1β. *Biochemistry* **28**, 6150-6156
38. Fujiwara, T. and Nagayama, K. (1989) Efficiency of heteronuclear broadband decoupling and homonuclear J cross polarization analyzed on two time scales. *J. Magn. Reson.* **81**, 245-254
39. Fujiwara, T. and Nagayama, K. (1988) Composite inversion pulses with frequency switching and their application to broadband decoupling. *J. Magn. Reson.* **77**, 53-63
40. Delagrio, F. (1993) *NMRPipe System of Software*, National Institute of Health, Bethesda
41. Garrett, D.S., Powers, R., Gronenborn, A.M., and Clore, G.M. (1991) A common sense approach to peak-picking in two-, three-, and four-dimensional spectra using automatic computer analysis of contor diagrams. *J. Magn. Reson.* **95**, 214-220
42. Wüthrich, K. (1986) *NMR of Proteins and Nucleic Acids*, Wiley-Interscience, New York
43. Chazin, W.J. and Wright, P.E. (1988) Complete assignment of ^{1}H nuclear magnetic resonance spectrum of french bean plastocyanin: Application of an integrated approach to spin system identification in proteins. *J. Mol. Biol.* **202**, 603-622
44. Wishart, D.S., Sykes, B.D., and Richards, F.M. (1991) Relationship between nuclear magnetic resonance chemical shift and protein secondary structure. *J. Mol. Biol.* **222**, 311-333
45. Wishart, D.S. and Sykes, B.D. (1994) Chemical shifts as a tool for structure determination. *Methods Enzymol.* **239**, 363-392
46. Gagné, S., Tsuda, S., Li, M.X., Chandra, M., Smillie, L.B., and Sykes, B.D. (1994) Quantification of the calcium-induced secondary structural changes in the regulatory domain of troponin-C. *Protein Sci.* **3**, 1961-1974
47. Ikura, M., Spera, S., Barbato, G., Kay, L.E., Krinks, M., and Bax, A. (1991) Secondary structure and side-chain ^{1}H and ^{13}C resonance assignments of calmodulin in solution by heteronuclear multidimensional NMR spectroscopy. *Biochemistry* **30**, 9216-9228
48. Wagner, G., Pardi, A., and Wüthrich, K. (1983) Hydrogen bond length and ^{1}H NMR chemical shifts in proteins. *J. Am. Chem. Soc.* **105**, 5948-5949
49. Serrano, L. and Fersht, A.R. (1989) Capping and α-helix stability. *Nature* **342**, 296-299
50. Bell, J.A., Becktel, W.J., Sauer, U., Basse, W.A., and Matthews, B.W. (1992) Dissection of helix capping in T4 lysozyme by structural and thermodynamic analysis of six amino acid substitutions at Thr59. *Biochemistry* **31**, 3591-3596
51. Matthews, B.W. (1993) Structural and genetic analysis of protein stability. *Annu. Rev. Biochem.* **62**, 139-160
52. Ikura, M., Clore, G.M., Gronenborn, A.M., Zhu, G., Klee, C.B.,

and Bax, A. (1992) Solution structure of a calmodulin-target peptide complex by multidimensional NMR. *Science* **256**, 632-638
53. Meador, W.E., Means, A.R., and Quiocho, F.A. (1992) Target enzyme recognition by calmodulin: 2.4 Å structure of a calmodulin-peptide complex. *Science* **257**, 1251-1255
54. Zhang, M., Li, M., Wang, J.H., and Vogel, H.J. (1994) The effect of Met→Leu mutations on calmodulin's ability to activate cyclic nucleotide phosphodiesterase. *J. Biol. Chem.* **269**, 15546-15552
55. Zhang, M. and Vogel, H.J. (1994) Two-dimensional NMR studies of selenomethyionyl-calmodulin. *J. Mol. Biol.* **239**, 545-554
56. Rees, D.C., Lewis, M., and Lipscomb, W.N. (1983) Refined crystal structure of carboxypeptidate A at 1.54 Å resolution. *J. Mol. Biol.* **168**, 367-387
57. Strynadka, N.C.J. and James, M.N.G. (1991) Towards an understanding of the effects of calcium on protein structure and function. *Curr. Opin. Struct. Biol.* **1**, 905-914
58. Li, M.X., Gagné, S., Tsuda, S., Kay, C.M., Smillie, L.B., and Sykes, B.D. (1995) Calcium binding to the regulatory N-domain of skeletal muscle troponin C occurs in a stepwise manner. *Biochemistry* **34**, 8330-8340
59. Grabarek, Z., Grabarek, J., Leavis, P.C., and Gergely, J. (1983) Cooperative binding to the Ca^{2+}-specific sites of troponin C in regulated actin and actomyosin. *J. Biol. Chem.* **258**, 14098-14102